RESEARCH ARTICLE | DECEMBER 09 2024

Magnetization reversal of perpendicular magnetic anisotropy multilayers on polymeric substrates for flexible spintronics applications

R. S. Bevan ; R. Chhatoi; S. Mallick ; C. Cafolla ; B. Nicholson; S. Bedanta ; D. Atkinson

J. Appl. Phys. 136, 223901 (2024)
https://doi.org/10.1063/5.0243189

Journal of Applied Physics | ARTICLE | pubs.aip.org/aip/jap

Magnetization reversal of perpendicular magnetic anisotropy multilayers on polymeric substrates for flexible spintronics applications

Cite as: J. Appl. Phys. 136, 223901 (2024); doi: 10.1063/5.0243189
Submitted: 9 October 2024 · Accepted: 18 November 2024 ·
Published Online: 9 December 2024

R. S. Bevan,[1] R. Chhatoi,[2] S. Mallick,[2] C. Cafolla,[1] B. Nicholson,[1] S. Bedanta,[2] and D. Atkinson[1,a)]

AFFILIATIONS

[1]Department of Physics, Durham University, Durham, United Kingdom
[2]Laboratory for Nanomagnetism and Magnetic Materials (LNMM), School of Physical Sciences, National Institute of Science Education and Research (NISER), Homi Bhabha National Institute (HBNI), Bhubaneswar, India

[a)]**Author to whom correspondence should be addressed:** del.atkinson@durham.ac.uk

ABSTRACT

Earlier demonstrations of spintronic functionality on flexible substrates have highlighted the potential for spintronics in flexible electronics applications. However, for device applications, the relationship between global magnetization reversal, as measured by hysteresis, and the local reversal processes of nucleation and growth of magnetic domains need to be understood for magnetic systems on flexible substrates. This study compares the local magnetization reversal behavior of perpendicularly magnetized Pt/CoFeB/Pt and Pt/Co/Pt on rigid and flexible polymeric substrates using magneto-optical Kerr effect magnetometry and microscopy. It is shown that while the magnetic hysteresis is comparable, the local details of the nucleation and field driven reversal are quite different and are attributed to the greater variability of the surface structures of the polymeric substrates, which has implications for consistency in device performance.

I. INTRODUCTION

The field of spintronics has grown significantly over the past decade with perpendicular magnetic anisotropy (PMA) forming a critical component of many systems, while rapid developments of spin–orbit torque (SOT) switching in thin film multilayers has led to the development of SOT magnetic random access memory (MRAM).[1–5] These spintronic applications are built upon multilayers grown and patterned on rigid substrates and integrated with silicon electronics using conventional CMOS compatible processing.

Beyond conventional electronics, there has been a huge expansion in research and development in flexible electronics. This is driven by their applications need for functionality that is low cost and has short design-to-manufacture timescales, which is being delivered with thin-film metal–oxide electronic materials[6] and microprocessor circuits.[7] Applications can also be extended by integrating other flexible substrate hosted components, such as sensors[8–10] and energy harvesting[11,12] for use in aerospace,[13] medical imaging, wearable and implantable electronics,[13–16] and the Internet-of-Things.[17–19]

The opportunities enabled by flexible electronics are also driving research in spintronics on polymeric substrates that ultimately may be integrated with flexible circuits. These developments bring the potential advantages of flexible substrates to spintronics, such as flexible non-planar form factor, strain-induced property changes, and sensing opportunities, but they must overcome the constraints imposed by the intrinsically higher surface roughness and topographical defects common in polymeric substrates compared to rigid silicon-based substrates. Substrate roughness is a key concern for spintronics as the requirement for PMA depends upon magnetic layers that are typically less than 1 nm thick, while the magnetization reversal, which involves nucleation, propagation, and pinning of domain walls, is sensitive to local variations and defects.

Early developments of spintronics on flexible substrates focused on Kapton®, a commercial polyimide (PI) widely used in flexible electronics, with studies demonstrating tunneling magnetoresistance in a relatively thick in-plane magnetized structure[20] and the development of PMA in Pt/CoFeB/Pt multilayers.[21] While early work also investigated the Pt/Co/MgO system grown on polyethylene naphthalate

(PEN), another important substrate for flexible electronics. In this case, the PEN surface was first planarized with an additional polymeric layer and the study established the development of PMA and SOT driven reversal.[22] These works highlight the commonly used multilayered PMA systems, where Pt is layered with ultrathin Co or CoFeB and PMA is established via interface effects.[23–26] In the case of CoFeB, the dilution of the ferromagnet with B tends to reduce the strength of the interface anisotropy,[27,28] which decreases the coercivity and can improve the switching efficiency.[29] More recent studies have reported a strain-mediated enhancement of the SOT in PMA Pt/Co on PI,[30] increased stability to strain in repeated Pt/Co multilayer stacks on polyvinylidene fluoride or polyvinylidene difluoride (PVDF),[31] and evidence of irreversible bending-induced anisotropy changes in Pt/Co/Pt on polyethylene terephthalate (PET).[32,33]

Here, the aim is to understand the local magnetization reversal of the common Pt/Co and Pt/CoFeB PMA systems on industry-relevant flexible polymeric substrates in comparison with the behavior observed for the same systems on rigid, smooth substrates via observations of domain nucleation and the pinning and propagation of domain walls during reversal. These two common magnetic systems have very different reversed domain nucleation densities, which in turn impacts the reversal processes. This study compares the large scale or "global" reversal behavior as shown via large area hysteresis measurements with domain images during the reversal process, which show the local variations in the magnetization states associated with the onset of reversal via nucleation and the propagation of domains.

There have been a few reports of domains visualized on PMA systems on various flexible substrates with some indications of the influence of the substrate[21,31,34] and other works showing the behavior under applied stress and strain on PI and PVDF[31] and PET.[32] This study shows a direct comparison of magnetization reversal at defined points through magnetic hysteresis via domain observations of PMA layered structures grown on Si/SiO_2 or on PI or PEN flexible substrates. The PEN is a commercially available substrate that incorporates a smoothing layer, and the PI is a spin-coated layer used in high-volume flexible electronics production.

II. EXPERIMENTAL DETAILS

The PI substrate was a nominal $4\,\mu m$ thick spin-coated layer adhered to a glass platen, enabling industrial wafer processing. The PEN substrate was Teonex®Q65H, which is colorless and primed on one side to create an "ultra smooth surface."[35] The thickness of the PEN[35] was $125\,\mu m$ and the thickness of SiO_2 on silicon was $150\,\mu m$. The Si/SiO_2 and PEN substrates were cleaned in an ultrasonic bath with acetone followed by isopropan-2-ol (IPA), while the PI substrates were cleaned only in the IPA, given their degradability in acetone. Multilayered thin-films consisting of Pt(5 nm)/CoFeB(0.7 nm)/Pt(3 nm) and Pt(3 nm)/Co(0.6 nm)/Pt(3 nm) were deposited by sputtering onto the substrates from a base pressure of $<1 \times 10^{-7}$ Torr at a working gas pressure of Ar of order 1×10^{-3} Torr and the growth rates were around 0.25 Å/s. Regarding the crystallographic structuring of the thin-films, previous studies have shown that the $Co_{40}Fe_{40}B_{20}$ alloy typically has an amorphous structure,[36] while the Pt and the ultrathin Co films will be composed of fcc-phase crystallites.[37,38] Structural analysis was undertaken with x-ray reflectivity (XRR) using a Cu-source Bruker D8 diffractometer to determine the multilayer structure and confirm the film thicknesses, the reflectivity data were analyzed using the GenX code.[39] Atomic force microscopy (AFM) was used to investigate the surface roughness and topographical structuring of the substrates. AFM imaging was performed in amplitude modulation,[40,41] in air at ambient conditions using a MFP-3D system (Oxford Instruments) with a HqNSC36/Cr/Au Bs cantilever, calibrated by the thermal method ($k = 2\,N/m$).[42] At least three different areas per sample were explored to ensure reproducibility. Magnetic hysteresis was measured with a laboratory built laser-based magneto-optical Kerr effect (MOKE) system, and domain imaging and hysteresis loops were obtained using an EVICO polar MOKE microscope,[43] enabling investigation of both the global magnetization states and imaging of the local nucleation and evolution of reversed domains as a function of the magnetic field.

III. RESULTS AND DISCUSSION

Figure 1 shows examples of AFM images of the three substrates before film deposition. As expected, the Si/SiO_2 wafer substrate, Fig. 1(a), is relatively smooth, with a few small topographical defects, likely associated with some surface debris contamination. The flexible substrates, Figs. 1(b) and 1(c), show stark contrast to the Si/SiO_2 substrate. For PI, Fig. 1(b), large linear topographical structures are clear in addition to particle-like features and regions of lower roughness (comparable to the Si/SiO_2 substrate). Topographical features are very pronounced on the PEN substrate, Fig. 1(c), showing a highly inhomogenous surface with multiple hollows and protrusions, as well as aggregates and indications of a multilayered structure. The global roughness of the substrates was obtained as the root mean square value of z-height values[44] (S_q), averaged over at least three images of different sizes, which gives 0.7 ± 0.3 nm for Si/SiO_2, 1.2 ± 0.4 nm for PI and 2.9 ± 0.9 nm for PEN.

Figure 2 shows examples of AFM images of four samples after film deposition. The topographical features and roughness of the thin films seem to depend not only on the substrate, but also on the type of deposited layers. CoFeB multilayers [Figs. 2(a) and 2(b)] presents a different topography in comparison to Co-based multilayers [Figs. 2(c) and 2(d)]. Interestingly, some of the topographical features of the films show a height of 20/25 nm, that is, greater than that of the thickness of the deposited layers but comparable to the height variation of some of the substrate features (18 nm, see Fig. 1). This suggests a conformal behavior of the deposited layers on the substrate defects. The qualitative analysis on the films topography is quantitatively confirmed by comparing their roughness. The roughness of the samples was obtained as the root mean square value of z-height values,[44] averaged over at least three images of different sizes, which gives 1.0 ± 0.4 nm for CoFeB when grown on Si/SiO_2 and 1.2 ± 0.5 nm when grown on PI; 3.7 ± 1.5 nm for Co-based layers grown on Si/SiO_2 and 5.1 ± 2.6 nm when grown on PEN. Using flexible substrates in comparison to rigid ones results in an overall increase in roughness and topographical variability for both CoFeB- and Co-based multilayers. Figure 3 shows specular XRR measurements and analysis for the same materials deposited onto Si/SiO_2 and on PI. The XRR analysis indicates a larger interface width between the substrate and the lower Pt layer

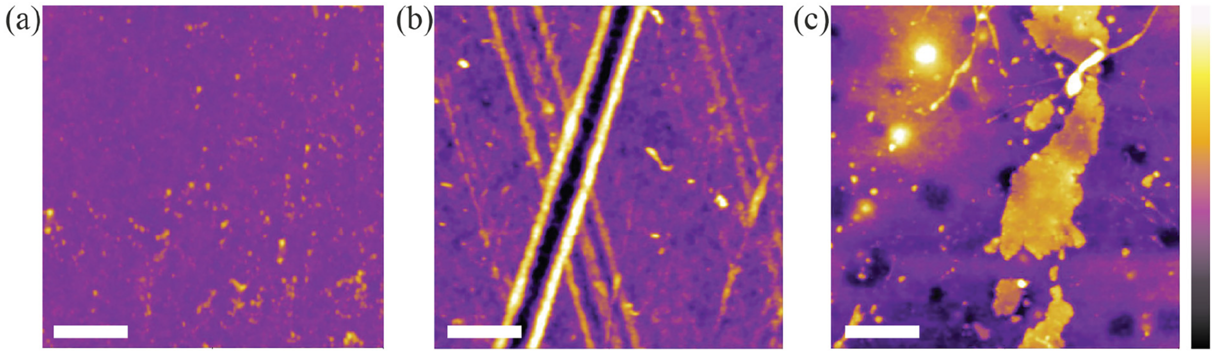

FIG. 1. Atomic force microscopy imaging of the three substrates tested here: (a) Si/SiO_2, (b) PI, and (c) PEN. While Si/SiO_2 shows a relatively homogeneous and flat surface, the flexible substrates present multiple topographical defects from particle-like features to crack lines. The scale bar represents 400 nm. The color scale bar represents a height variation of 18 nm.

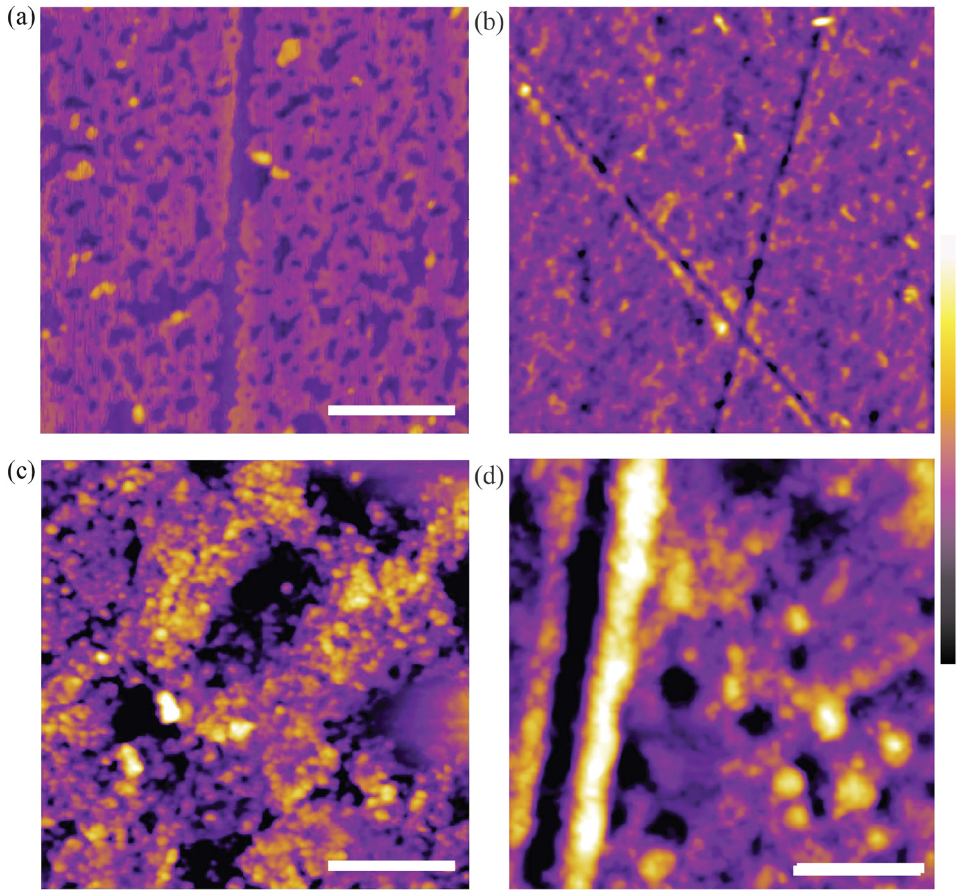

FIG. 2. Atomic force microscopy imaging of the four samples: Pt(5)/CoFeB(0.7)/Pt(5) grown on (a) Si/SiO_2 and (b) PI; and Pt(3)/Co(0.6)/Pt(3) on (c) Si/SiO_2 and (d) PEN substrates. The topography of the films is the result of a complex interplay between the substrates and the deposited multilayers. For both CoFeB and Co-based samples, the use of flexible substrates increases topographical defects and roughness in the final films, as shown by deeper crack lines in (b) and (d) in comparison to (a) and (c). The scale bar represents 400 nm. The color scale bar represents a height variation of 25 nm.

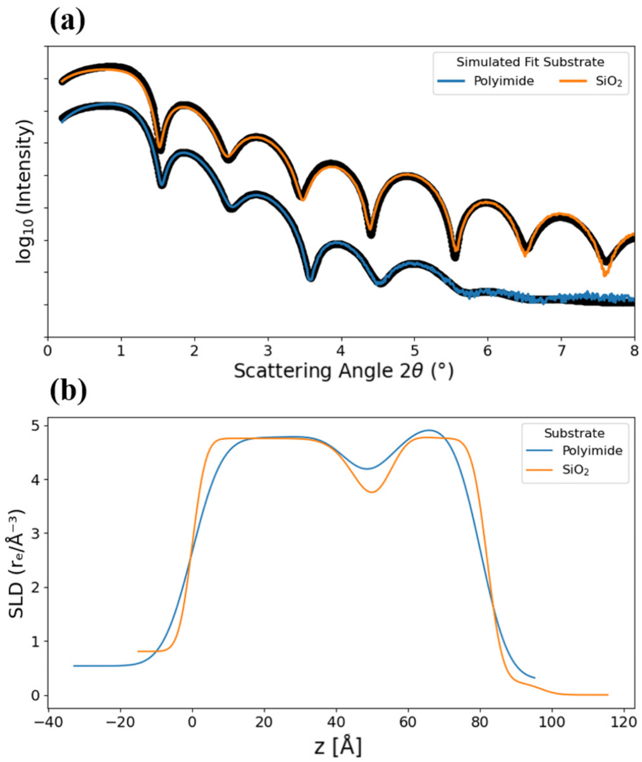

FIG. 3. (a) Specular x-ray reflectivity measured for the same Pt, CoFeB, and Pt layers sputter deposited onto SiO_2 and polyimide substrates, respectively. The solid lines through the data points represent the best fitting models obtained using the GenX code.[39] The data for the two samples are offset on the y-axis for clarity. (b) A comparison of the scattering length density (SLD) profiles, obtained from the best-fitting simulations in (a) for the Pt/CoFeB/Pt layers on SiO_2 and polyimide substrates.

and the Pt and FM layer interfaces for the polymer, consistent with higher roughness from the AFM.

Magnetic hysteresis loops confirm out-of-plane magnetic anisotropy and a remanence ratio, M_r/M_s of ∼1.0. Figure 4 presents hysteresis from MOKE microscopy showing that the multilayers grown on flexible substrates have comparable, but not identical magnetization reversal, to those grown on Si/SiO_2. For the Co-based multilayers, Figs. 4(c) and 4(d), the coercivity is approximately eight times larger than for the CoFeB multilayers [Figs. 4(a) and 4(b)], which may be attributed to lower interfacial anisotropy due to B dilution. The impact of the flexible substrate on the overall reversal is not simply to increase or decrease the reversal field. The CoFeB-based multilayer on PI shows a slightly higher coercivity than on Si/SiO_2, but with a broader field-driven reversal, while the Co-based multilayer on PEN has a coercivity that is ∼25% smaller and the onset of reversal less sharp than the equivalent system on Si/SiO_2.

Figures 5 and 6 show magnetic domain images for CoFeB and Co-based systems, respectively, at key points during magnetization reversal. The images labeled 1 and 5 show the magnetic contrast at nominal positive and negative saturation. Images labeled 2 show the magnetic contrast soon after the onset of reversal, while images 3 and 6 show the domain structure at approximately zero net magnetization on opposite sides of the hysteresis loop. At large positive and negative magnetic fields, the magnetic contrast is uniformly dark or light, indicating the systems are magnetically saturated, with exceptions for CoFeB on PI and Co on PEN at large negative fields, where some small contrast features are present, which may represent imperfect corrections of the structural contrast.

The magnetic contrast resulting from the onset of reversal, shown in the images labeled 2, highlights the critical difference between these thin-film systems grown on rigid Si/SiO_2 and on flexible polymeric substrates. The images also show significant differences between the CoFeB and Co systems on Si/SiO_2. The onset of reversal involves the nucleation of bubble domains, bounded by roughly circular domain walls, which are characteristic of high quality films with uniform PMA;[45–47] however, the density of first onset nucleation centers is quite different between the CoFeB and Co multilayered systems, with a nucleation density of $<1\,\text{point/mm}^2$ for CoFeB and $>100\,\text{point/mm}^2$ for Co, with reversal of the Co system driven by high density uniform domain nucleation compared to the nucleation and rapid growth of a much smaller numbers of bubble domains in the CoFeB system.

These results can be understood in terms of the higher anisotropy in the Co system, evidenced by the larger coercivity, which may dominate any small local energy variations compared to the effect of such variations in the weaker PMA CoFeB system. In both cases, with increasing field the domain walls move outward as these bubble domains expand and coalesce as reversal progresses.

The onset and progression of reversal for the CoFeB and Co systems on flexible substrates [Figs. 5(b) and 6(b)] are different to the observations of these systems on the Si/SiO_2 substrates. In the case of CoFeB on PI, the number of domains nucleated per unit area is similar to the CoFeB on Si/SiO_2, which may be associated with the lower roughness regions and indicates that the rougher PI substrate does not notably modify the nucleation process. However, for the CoFeB system on PI, the reverse domains nucleated are not circular but are enclosed by jagged domain walls with large linear components in some directions. With increasing field, the domain expansion is not isotropic but clearly constrained by some of these linear features that are associated with structures of the PI substrate. At the highest fields, the system becomes uniformly magnetized. In the case of the Co system on PEN, the reversal is characterized by magnetic contrast that is dominated by the influence of geometrical features associated with the substrate. For the Co-based system on Si/SiO_2, reversal is characterized by many circular reverse domains nucleated uniformly across the substrate and on PEN, the onset of magnetization reversal is characterized by magneto-optical contrast that is associated with linear features associated with the substrate. With increasing field, the extent of the reversed magnetization increases but evidence of domain wall expansion is not clear for this system on PEN. In all cases, the magnetic reversal behavior is consistently similar for equivalent positive and negative fields and between field cycles, with domain nucleation and growth occurring at the same sites on both field directions, as seen by comparison of domains in images 3 and 6 in Figs. 5(a), 5(b), 6(a), and 6(b) at positive and negative coercive points.

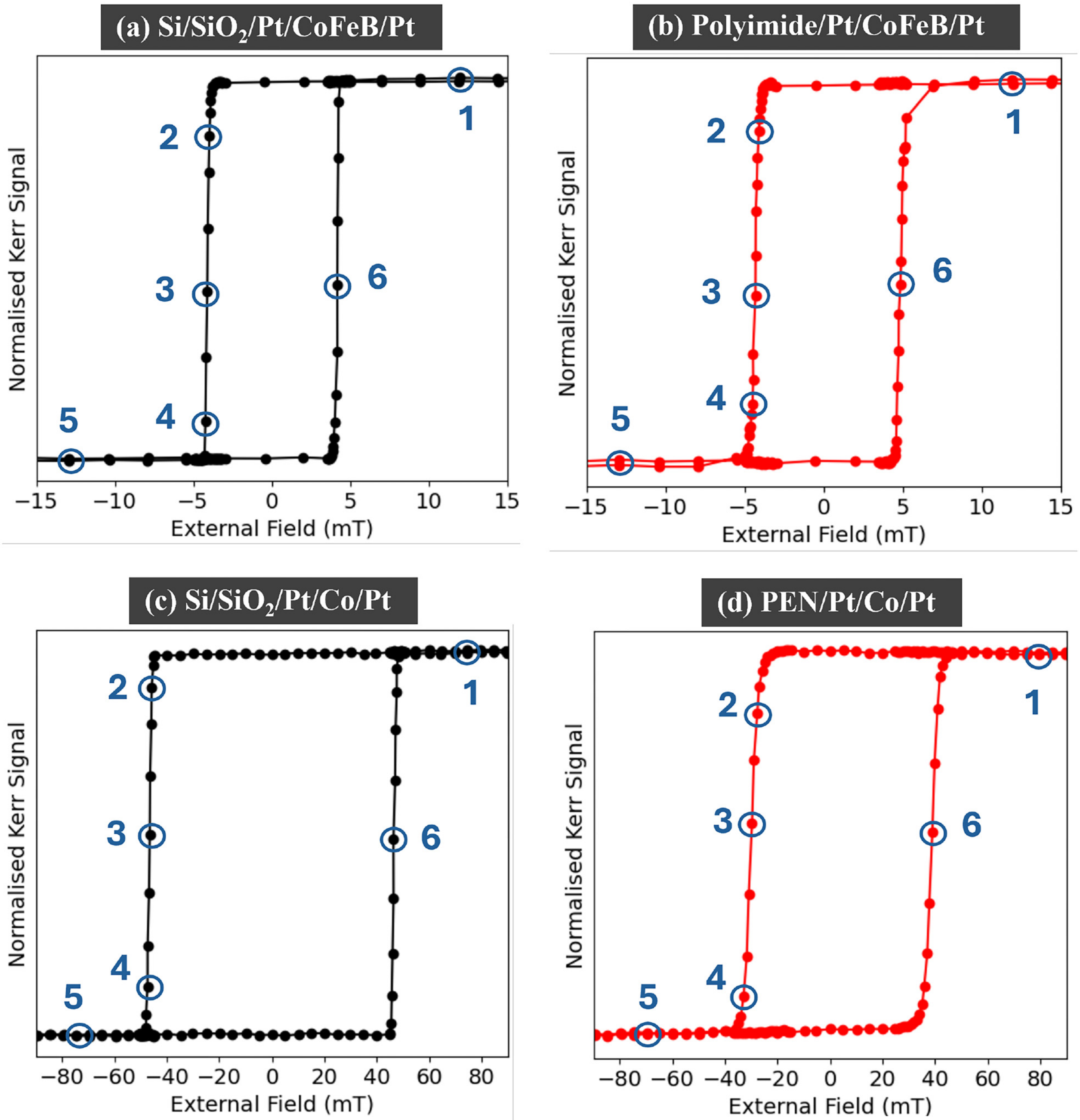

FIG. 4. Polar MOKE microscopy measurements of Pt(5)/CoFeB(0.7)/Pt(5) on (a) Si/SiO$_2$ and (b) PI and of Pt(3)/Co(0.6)/Pt(3) on (c) Si/SiO$_2$ and (d) PEN substrates. The data were measured to ± 45 and ± 100 mT for CoFeB and Co, respectively, but truncated for presentation. The circled points relate to domain images in Figs. 3 and 4.

Overall, the results show that the reversal depends on both the magnetic thin-film system and the polymeric substrate. For the CoFeB system, the nucleation of reverse domains is not strongly affected by the PI substrate. However, the growth of the reversed domains, which dominates the magnetization reversal of this system, is constrained by substrate features, indicating that the substrate imposes variations on the energy landscape that affects the domain wall propagation and pinning, which slightly

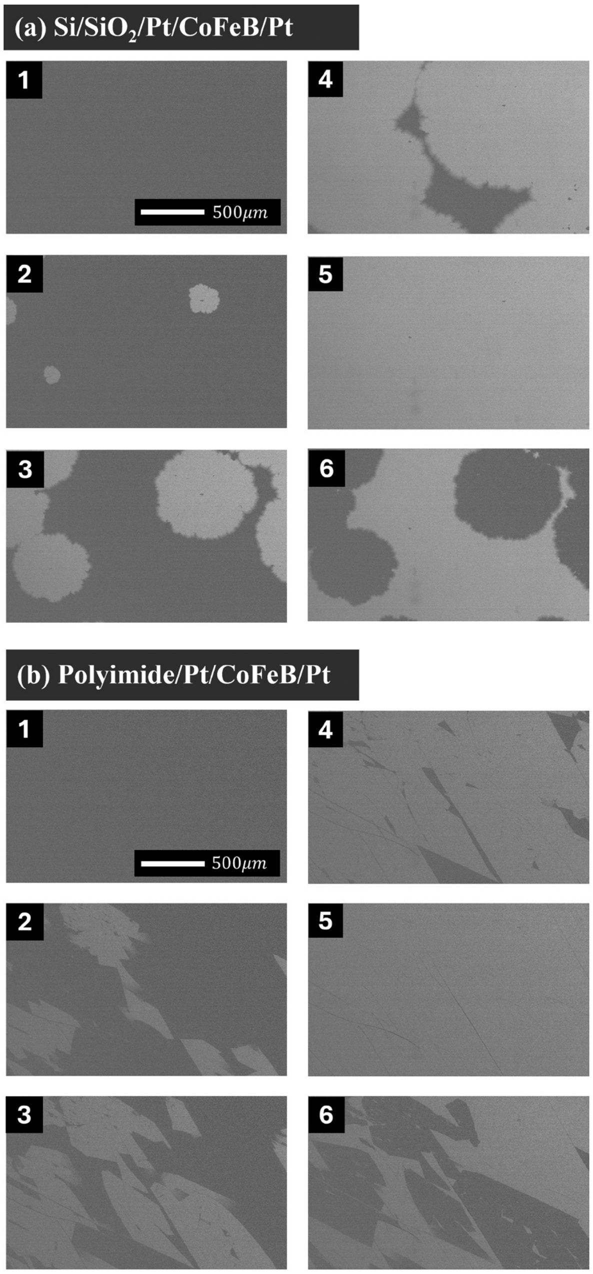

FIG. 5. Comparison of magnetization reversal domain behavior of Pt(5 nm)/CoFeB(0.7 nm)/Pt(3 nm) multilayers on (a) Si/SiO$_2$ substrate and (b) PI substrate. The numbers 1–6 relate the domain images to the points on the corresponding hysteresis loop in Fig. 2.

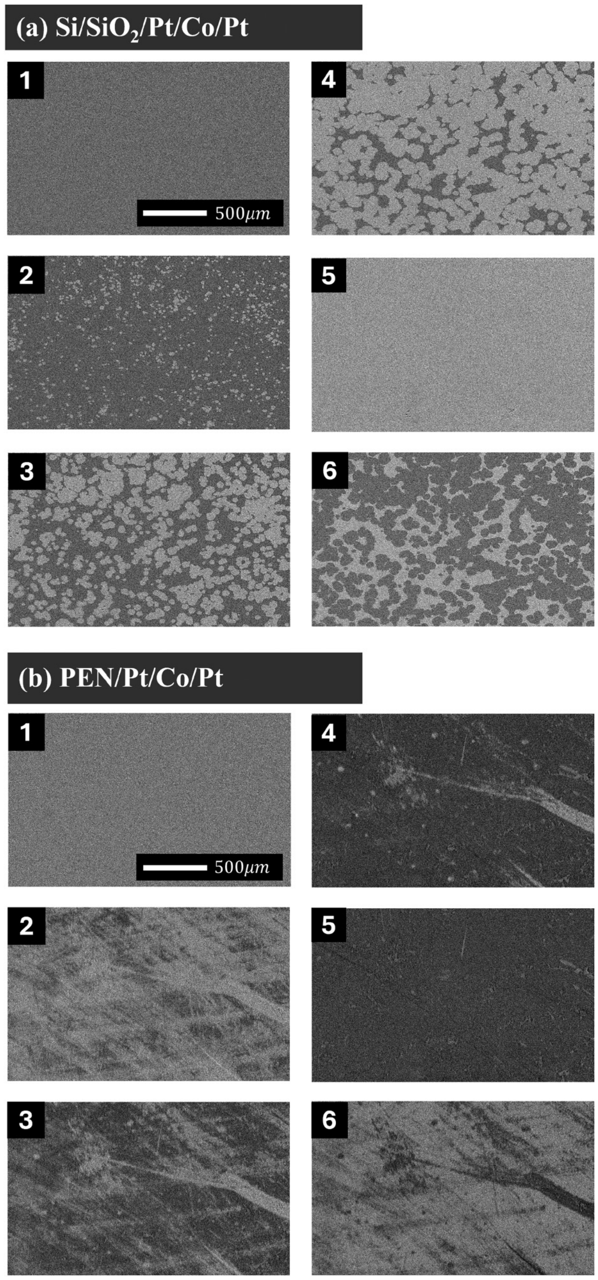

FIG. 6. Comparison of magnetization reversal domain behaviors of Pt(3 nm)/Co(0.6 nm)/Pt(3 nm) multilayers on (a) Si/SiO$_2$ substrate and (b) PEN substrate. The numbers 1–6 relate the domain images to the points on the corresponding hysteresis loop in Fig. 2.

increases the coercivity. For the higher switching field Co system, the PEN substrate significantly changes the observed behavior, in this case, the reversal is dominated by the nucleation of reversed magnetization and the observed reversed magnetization is constrained by substrate features; in this case, the substrate modifies the energy landscape such that the nucleation dominated reversal processes occur at lower energy resulting in a reduced coercivity.

IV. SUMMARY AND CONCLUSIONS

In this work, we have examined the effect that flexible substrates have on the magnetization switching of perpendicularly anisotropic thin film Pt/Co and Pt/CoFeB multilayers. It is found that global switching is comparable for all substrates from an analysis of hysteresis, but this masks significant difference in details of the magnetization reversal associated with the substrate. Overall, the differences in the magnetization reversal between the polymeric substrates and the smoother Si/SiO_2 may be attributed to differences in the topographical roughness of the different surfaces. The differences between the CoFeB and Co systems on PI and PEN are also associated with the differences in topographical features and roughness, but may also be linked to the different strength of PMA within these two magnetic systems. These results highlight the need to consider the details of the local reversal process for applications of spintronic multilayers on flexible substrates.

ACKNOWLEDGMENTS

The authors thank Ala Safaaldin Bahaaldin for fabricating the Pt(3)/Co(0.6)/Pt(3) samples. Funding from the Royal Society International Exchange scheme with NISER, Bhubaneswar, India (No. IES\R1\201331) is acknowledged.

AUTHOR DECLARATIONS

Conflict of Interest

The authors have no conflicts to disclose.

Author Contributions

R. S. Bevan: Data curation (equal); Formal analysis (equal); Investigation (equal); Methodology (equal); Project administration (supporting); Writing – original draft (lead); Writing – review & editing (supporting). **R. Chhatoi:** Data curation (equal); Investigation (equal); Methodology (equal); Visualization (equal); Writing – review & editing (supporting). **S. Mallick:** Data curation (equal); Investigation (equal); Methodology (equal); Writing – review & editing (equal). **C. Cafolla:** Formal analysis (equal); Investigation (equal); Methodology (equal); Visualization (equal); Writing – original draft (supporting); Writing – review & editing (equal). **B. Nicholson:** Investigation (equal); Methodology (equal); Supervision (supporting); Visualization (supporting); Writing – original draft (supporting); Writing – review & editing (equal). **S. Bedanta:** Conceptualization (supporting); Funding acquisition (equal); Project administration (equal); Resources (equal); Supervision (lead); Writing – original draft (supporting); Writing – review & editing (equal). **D. Atkinson:** Conceptualization (lead); Funding acquisition (equal); Investigation (equal); Methodology (equal); Project administration (equal); Resources (equal); Supervision (lead); Writing – original draft (lead); Writing – review & editing (lead).

DATA AVAILABILITY

The data that support the findings of this study are available from the corresponding author upon reasonable request.

REFERENCES

[1] H. Lin, X. Luo, L. Liu, D. Wang, X. Zhao, Z. Wang, X. Xue, F. Zhang, and G. Xing, "All-electrical control of compact SOT-MRAM: Toward highly efficient and reliable non-volatile in-memory computing," Micromachines **13**, 319 (2022).
[2] K. Cai, G. Talmelli, K. Fan, S. Van Beek, V. Kateel, M. Gupta, M. Monteiro, M. B. Chroud, G. Jayakumar, A. Trovato *et al.*, "First demonstration of field-free perpendicular SOT-MRAM for ultrafast and high-density embedded memories," in *2022 International Electron Devices Meeting (IEDM)* (IEEE, 2022), pp. 36–42.
[3] M. Natsui, A. Tamakoshi, H. Honjo, T. Watanabe, T. Nasuno, C. Zhang, T. Tanigawa, H. Inoue, M. Niwa, T. Yoshiduka *et al.*, "Dual-port SOT-MRAM achieving 90-MHz read and 60-MHz write operations under field-assistance-free condition," IEEE J. Solid-State Circuits **56**, 1116–1128 (2020).
[4] K. Garello, F. Yasin, H. Hody, S. Couet, L. Souriau, S. H. Sharifi, J. Swerts, R. Carpenter, S. Rao, W. Kim *et al.*, "Manufacturable 300 mm platform solution for field-free switching SOT-MRAM," in *2019 Symposium on VLSI Circuits* (IEEE, 2019), pp. T194–T195.
[5] K. Garello, F. Yasin, S. Couet, L. Souriau, J. Swerts, S. Rao, S. Van Beek, W. Kim, E. Liu, S. Kundu *et al.*, "SOT-MRAM 300 mm integration for low power and ultrafast embedded memories," in *2018 IEEE Symposium on VLSI Circuits* (IEEE, 2018), pp. 81–82.
[6] J. Troughton and D. Atkinson, "Amorphous InGaZnO and metal oxide semiconductor devices: An overview and current status," J. Mater. Chem. C **7**, 12388–12414 (2019).
[7] J. Biggs, J. Myers, J. Kufel, E. Ozer, S. Craske, A. Sou, C. Ramsdale, K. Williamson, R. Price, and S. White, "A natively flexible 32-bit arm microprocessor," Nature **595**, 532–536 (2021).
[8] Z. Dong, Z. Gong, B. Chen, T. Sheng, Y. Cao, Q. He, P. Zhao, and Y. Jiang, "Ultra-thin flexible skin with all-polyimide pressure and airflow sensor array for estimation of flight parameters," IEEE Sens. J. **23**, 29494–29501 (2023).
[9] W. Xiong, C. Zhu, D. Guo, C. Hou, Z. Yang, Z. Xu, L. Qiu, H. Yang, K. Li, and Y. Huang, "Bio-inspired, intelligent flexible sensing skin for multifunctional flying perception," Nano Energy **90**, 106550 (2021).
[10] C. Voigt, S. Mosch, E. S. Oliveros-Mata, D. Makarov, C. Schubert, M. Ott, T. Preußner, and M. Vinnichenko, "Printed anisotropic magnetoresistive sensors on flexible polymer foils," in *Proceedings MDPI* (MDPI, 2024), Vol. 97, p. 177.
[11] Y. Hu, T. Niu, Y. Liu, Y. Zhou, Y. Xia, C. Ran, Z. Wu, L. Song, P. Muller-Buschbaum, Y. Chen, and W. Huang, "Flexible perovskite solar cells with high power-per-weight: Progress, application, and perspectives," ACS Energy Lett. **6**, 2917–2943 (2021).
[12] M. Saravanapavanantham, J. Mwaura, and V. Bulović, "Printed organic photovoltaic modules on transferable ultra-thin substrates as additive power sources," Small Methods **7**, 2200940 (2023).
[13] D. Corzo, G. Tostado, and D. Baran, "Flexible electronics: Status, challenges and opportunities," Front. Electron. **1**, 594003 (2020).
[14] L. Wang, K. Jiang, and G. Shen, "Wearable, implantable, and interventional medical devices based on smart electronic skins," Adv. Mater. Technol. **6**, 2100107 (2021).
[15] L. Wang, K. Jiang, and G. Shen, "A perspective on flexible sensors in developing diagnostic devices," Appl. Phys. Lett. **119**, 150501 (2021).
[16] M. Ha, G. S. Cañón Bermúdez, T. Kosub, I. Mönch, Y. Zabila, E. S. Oliveros Mata, R. Illing, Y. Wang, J. Fassbender, and D. Makarov, "Printable and stretchable giant magnetoresistive sensors for highly compliant and skin-conformal electronics," Adv. Mater. **33**, 2005521 (2021).
[17] Y. Zhan, Y. Mei, and L. Zheng, "Materials capability and device performance in flexible electronics for the internet of things," J. Mater. Chem. C **2**, 1220–1232 (2014).
[18] G. Liu, Q. Tan, H. Kou, L. Zhang, J. Wang, W. Lv, H. Dong, and J. Xiong, "A flexible temperature sensor based on reduced graphene oxide for robot skin used in internet of things," Sensors **18**, 1400 (2018).
[19] Q. Shi, B. Dong, T. He, Z. Sun, J. Zhu, Z. Zhang, and C. Lee, "Progress in wearable electronics/photonics—Moving toward the era of artificial intelligence and internet of things," InfoMat **2**, 1131–1162 (2020).

[20]A. Bedoya-Pinto, M. Donolato, M. Gobbi, L. E. Hueso, and P. Vavassori, "Flexible spintronic devices on Kapton," Appl. Phys. Lett. **104**, 062412 (2014).
[21]T. Vemulkar, R. Mansell, A. Fernández-Pacheco, and R. Cowburn, "Toward flexible spintronics: Perpendicularly magnetized synthetic antiferromagnetic thin films and nanowires on polyimide substrates," Adv. Funct. Mater. **26**, 4704–4711 (2016).
[22]O. Lee, L. You, J. Jang, V. Subramanian, and S. Salahuddin, "Flexible spin-orbit torque devices," Appl. Phys. Lett. **107**, 252401 (2015).
[23]G. J. Lim, W. Gan, and W. S. Lew, "Effect of seed and interlayer Pt thickness on spin-orbit torque efficiency in Co/Pt multilayer with perpendicular magnetic anisotropy," J. Phys. D: Appl. Phys. **53**, 505002 (2020).
[24]L. Cestarollo, K. Srinivasan, and A. El-Ghazaly, "Investigation of perpendicular magnetic anisotropy in Pt/$Co_{20}Fe_{60}B_{20}$/Pt multi-layer structures," J. Magn. Magn. Mater. **562**, 169825 (2022).
[25]C. Yan, L. Chen, K. Zhou, L. Yang, Q. Fu, W. Wang, W.-C. Yue, L. Liang, Z. Tao, J. Du, Y.-L. Wang, and R. Liu, "Thickness-dependent magnetic properties in Pt/[Co/Ni] n multilayers with perpendicular magnetic anisotropy," Chin. Phys. B **32**, 017503 (2023).
[26]W. Du, M. Liu, G. Wang, H. Su, B. Liu, H. Meng, and X. Tang, "Stack structure and CoFeB composition dependence of perpendicular magnetic anisotropy employing Pt heavy metal layer," J. Alloys Compd. **928**, 167205 (2022).
[27]J. Zhang, Y. Zhao, P. Dou, W. Peng, H. Huang, X. Deng, Y. Wang, J. Liu, J. Xu, T. Zhu *et al.*, "Controllable spin–orbit torque induced by interfacial ion absorption in Ta/CoFeB/MgO multilayers with canted magnetizations," ACS Appl. Mater. Interfaces **15**, 49902–49910 (2023).
[28]A. Natarajarathinam, R. Zhu, P. Visscher, and S. Gupta, "Perpendicular magnetic tunnel junctions based on thin CoFeB free layer and Co-based multilayer synthetic antiferromagnet pinned layers," J. Appl. Phys. **111**, 07C918 (2012).
[29]Z. A. Bekele, R. Li, Y. Li, Y. Cao, X. Liu, and K. Wang, "Tuning the high-efficiency field-free current-induced deterministic switching via ultrathin PtMo layer with Mo content," Adv. Electron. Mater. **7**, 2100528 (2021).
[30]G. D. Hwee Wong, Z. Xu, W. Gan, C. C. I. Ang, W. C. Law, J. Tang, W. Zhang, P. K. J. Wong, X. Yu, F. Xu *et al.*, "Strain-mediated spin–orbit torque enhancement in Pt/Co on flexible substrate," ACS Nano **15**, 8319–8327 (2021).
[31]M. Li, H. Yang, Y. Xie, K. Huang, L. Pan, W. Tang, X. Bao, Y. Yang, J. Sun, X. Wang, S. Che, and R.-W. Li, "Enhanced stress stability in flexible Co/Pt multilayers with strong perpendicular magnetic anisotropy," Nano Lett. **23**, 8073–8080 (2023).
[32]J. Kim and J. Dho, "Bending strain–induced changes in perpendicular magnetic properties of Pt/Co/Pt films on flexible substrates," Appl. Phys. Lett. **124**, 102401 (2024).
[33]E. Pandey, B. B. Singh, P. Sharangi, and S. Bedanta, "Strain engineered domain structure and their relaxation in perpendicularly magnetized Co/Pt deposited on flexible polyimide," Nano Express **1**, 010037 (2020).
[34]S. Eimer, H. Cheng, J. Li, X. Zhang, C. Zhao, and W. Zhao, "Perpendicular magnetic anisotropy based spintronics devices in Pt/Co stacks under different hard and flexible substrates," Sci. China Inf. Sci. **66**, 122408 (2023).
[35]See https://www.tekra.com/sites/default/files/downloads/Tekra-Polyester-Films-Brochure-Web-Version.pdf for "DuPont Teijin Films, Tekra Brochure" (last accessed August 11, 2024.
[36]Y. Saito, N. Tezuka, S. Ikeda, and T. Endoh, "Large spin Hall effect and increase in perpendicular magnetic anisotropy in artificially synthesized amorphous W/Hf multilayer/CoFeB system," Appl. Phys. Lett. **116**, 132401 (2020).
[37]M. Tokaç, S. A. Bunyaev, G. N. Kakazei, D. S. Schmool, D. Atkinson, and A. T. Hindmarch, "Interfacial structure dependent spin mixing conductance in cobalt thin films," Phys. Rev. Lett. **115**, 056601 (2015).
[38]Y. Saito, S. Ikeda, and T. Endoh, "Synthetic antiferromagnetic layer based on Pt/Ru/Pt spacer layer with 1.05 nm interlayer exchange oscillation period for spin–orbit torque devices," Appl. Phys. Lett. **119**, 142401 (2021).
[39]M. Björck and G. Andersson, "Genx: An extensible x-ray reflectivity refinement program utilizing differential evolution," J. Appl. Crystallogr. **40**, 1174–1178 (2007).
[40]R. Garcıa and R. Perez, "Dynamic atomic force microscopy methods," Surf. Sci. Rep. **47**, 197–301 (2002).
[41]C. Cafolla, T. Bui, T. T. B. Le, A. Zen, W. J. Tay, A. Striolo, A. Michaelides, H. C. Greenwell, and K. Voïtchovsky, "Local probing of the nanoscale hydration landscape of kaolinite basal facets in the presence of ions," Mater. Today Phys. **46**, 101504 (2024).
[42]H.-J. Butt and M. Jaschke, "Calculation of thermal noise in atomic force microscopy," Nanotechnology **6**, 1 (1995).
[43]*Evico Magnetics Kerr Microscope Brochure* (2020).
[44]C. M. Mate and R. W. Carpick, *Tribology on the Small Scale: A Modern Textbook on Friction, Lubrication, and Wear*, Oxford Graduate Texts (Oxford University Press, 2019), ISBN: 9780199609802.
[45]J. Dho, "Ferromagnetic layer thickness dependence of magnetic domain structure in ultrathin symmetric Ta/Pt/Co/Pt/Ta multilayers," IEEE Trans. Magn. **58**, 1–5 (2022).
[46]M. Sharma, B. Ojha, S. Mohanty, S. Pütter, and S. Bedanta, "Study of domain wall dynamics in Pt/Co/Pt ultrathin films," Indian J. Phys. **98**, 1–7 (2024).
[47]N. Novakovic-Marinkovic, M.-A. Mawass, O. Volkov, P. Makushko, W. D. Engel, D. Makarov, and F. Kronast, "From stripes to bubbles: Deterministic transformation of magnetic domain patterns in Co/Pt multilayers induced by laser helicity," Phys. Rev. B **102**, 174412 (2020).